Journal Pre-proofs

Study on the behavior of squared and sub-rectangular tunnels using the Hyperstatic Reaction Method

Do Ngoc Anh, Dias Daniel, Zixin Zhang, Xin Huang, Nguyen Tai Tien, Pham Van Vi, Ouahcène Nait-Rabah

Please cite this article as: D. Ngoc Anh, D. Daniel, Z. Zhang, X. Huang, N. Tai Tien, P. Van Vi, O. Nait-Rabah, Study on the behavior of squared and sub-rectangular tunnels using the Hyperstatic Reaction Method, *Transportation Geotechnics* (2020), doi: https://doi.org/10.1016/j.trgeo.2020.100321

Study on the behavior of squared and sub-rectangular tunnels using the Hyperstatic Reaction Method

Do Ngoc Anh[1], Dias Daniel[2,3], Zixin Zhang[4,5], Xin Huang[4,5], Nguyen Tai Tien[1], Pham Van Vi[1], Ouahcène Nait-Rabah[6]

[1] Department of Underground and Mining Construction, Faculty of Civil Engineering, Hanoi University of Mining and Geology, Vietnam

[2] Professor, School of Automotive and Transportation Engineering, Hefei Univ. of Technology, Hefei 230009, China

[3] Geotechnical expert, Antea Group, Antony, France. (Corresponding author) ORCID: 0000-0003-2238-7827. Email:Daniel.dias@anteagroup.com

[4] Department of Geotechnical Engineering, Tongji University, 1239 Siping Road, Shanghai 200092, China

[5] Key Laboratory of Geotechnical and Underground Engineering of the Ministry of Education, Tongji University, Shanghai 200092, China

[6] UMR EcoFoG, Université de Guyane, Kourou, France

Abstract

Circular tunnels are usually encountered when excavating in weak soil medium at shallow depth and using shield machines. However, special shaped tunnels such as squared tunnels and sub-rectangular tunnels are also recently used to improve the efficiency of underground space use. This paper focuses on improving the performance of the Hyperstatic Reaction Method (HRM), which is a numerical method, for the case of squared or sub-rectangular tunnels. Special attention is paid to the tunnel shape influence by using various tunnel wall radii. The numerical HRM model was validated based on a comparison with the finite element method (FEM). The results indicated that HRM can be effectively used to estimate the behavior of squared or sub-rectangular tunnels. Then a parametric study was conducted to highlight the influence of the earth pressure coefficient and of the soil Young's modulus on the structural forces, and deformations induced by the excavation in the tunnel lining.

Keywords: Finite element method; tunnel; lining; squared shape; sub-rectangular shape.

1. Introduction

A circular shape is usually chosen for tunnels when they are excavated by a shield machine through weak soil mediums and at shallow depth. However, the main disadvantage of a circular tunnel is its small space utilization ratio. Special-shaped tunnels with cross-section shape between a circle and a rectangle can have a higher space utilization efficiency than a circular tunnel. It can also avoid stress concentration at the four corners, and thus have a greater bearing capacity compared with rectangular tunnels [11]. Special shaped tunnels such as squared

tunnels or sub-rectangular tunnels are therefore recently used to improve the efficiency of the underground space use [8,19]. The structural behavior of the segmental lining of shield tunnels was investigated through structural tests using either full-scale or reduced-scale specimens [7,20,21]. Kashima et al. [6] performed loading tests on a full segmental ring to assess the performance of the shield tunneling method. Blom [1] conducted full-scale loading tests for the Green Heart Tunnel in Holland. Nakamura et al. [11] reported full-scale loading tests on segmental linings, which assess the design adequacy for the world's first double track shield tunnel in Kyoto, Japan. Molins and Arnau [10] conducted in-situ full-scale tests on the segmental linings of Barcelona's new metro Line 9. The full-ring prototype loading tests can overcome the scale effects, check the mechanical integrity, and simulate different assemblage patterns and hydrogeological conditions. Zhang, et al. [19] carried out a 1:1 prototype loading method for special-shaped segmental lining, which investigated the mechanical behavior of the segments under designed loads. They have shown the influence of the lateral earth pressure coefficient. In particular, the role of the self-weight in the internal forces and deformation distributions of the segmental lining under shallow overburden conditions was explored. Due to the flatness of arches along the tunnel boundary, the arching effect on the squared or sub-rectangular tunnel is lower than on circular ones. As a consequence, structural forces and deformation induced in the tunnel lining are different for a special-shape tunnel.

As a new type of cross-section, the mechanical behavior of squared or sub-rectangular tunnel is not yet thoroughly evaluated, neither in terms of calculation method nor in terms of structural design [8,19]. To assess the rationale behind the full-scale tests, the values of resultant earth-water force around a tunnel lining at different burial depths need to be determined from a numerical model, especially for squared or sub-rectangular tunnels.

Recently, the Hyperstatic Reaction Method (HRM), which is part of the numerical method category, has been successfully applied to determine the behaviour of circular tunnel's lining [3,4] and [12-16]. One of the main advantages of the HRM is to permit a quick estimation of the tunnel lining behavior. This paper focuses on improving the performance of the HRM for the case of squared and/or sub-rectangular tunnels. Special attention is paid to the tunnel shape change by using various radii of the parts along the tunnel boundary. The numerical HRM model was validated based on a comparison with calculations using a finite element method (FEM). The results indicated that HRM can be effectively used to estimate the behavior of squared and/or sub-rectangular tunnels. Using the HRM model, a parametric study was conducted to highlight the influence of some parameters (earth pressure coefficient and soil Young's modulus) on the structural forces and deformations induced in the tunnel lining by the tunnel excavation.

2. Fundamental of HRM

The HRM method is based on the Finite Element Method (FEM) in which the tunnel lining is simulated by mono-dimensional elements that are able to estimate bending moments, axial forces and shear forces (see Figure 1). The presence of ground surrounding the tunnel is

modeled through normal and tangential springs connected to the nodes of the lining structure. Ground loads are considered as active pressures applied on the tunnel lining, which will be applied on the lining through normal and tangential springs. In the HRM model, once the displacement components of the nodes of the discretized structure are determined, it is possible to estimate the structural forces and displacement induced in each element and therefore also along the entire support structure. The evaluation of the unknown displacements is made through the global stiffness matrix definition of the entire structure and of its connections to the surrounding ground [5].

Details of the numerical HRM approach applied to the circular tunnel were introduced in the work of Oreste [12] and Do et al. [3]. Basically, while a unique radius is adopted for circular tunnels, different radii are used for the lining parts along the tunnel boundary in the case of squared and sub-rectangular tunnels. Unlike the sub-rectangular tunnel where the width and the height of the tunnel are different from each other, these dimensions are similar in the case of squared tunnel. The variation of radius between the lining parts along the tunnel boundary causes the change in the lining - soil interaction in terms of reaction forces acting from the soil to the tunnel lining. In this study, some significant modifications were proposed to extend the application of the HRM model to squared and sub-rectangular tunnels.
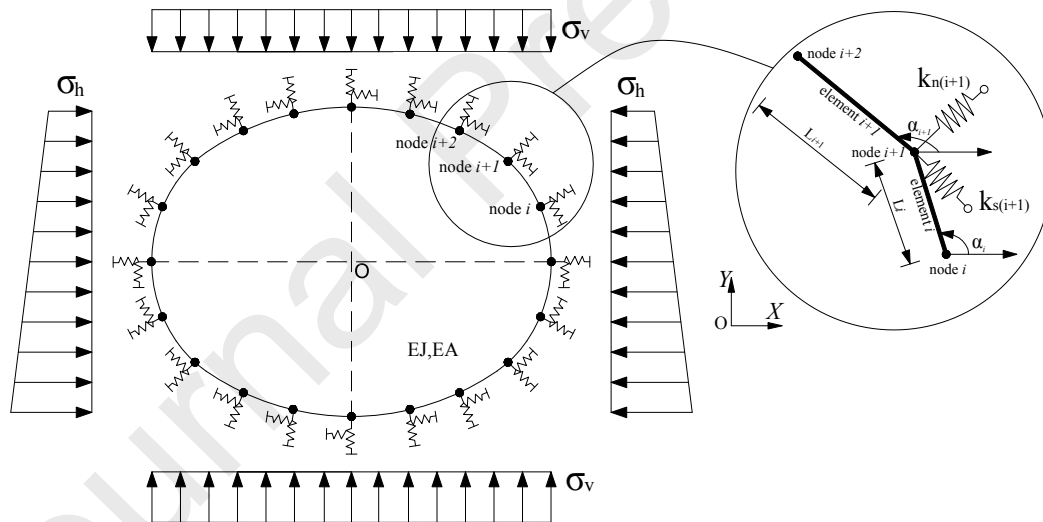
Figure 1. Calculation scheme of support structures with the HRM. With: σ_v: the vertical loads; σ_h: the horizontal loads; k_n: normal stiffness of springs; k_s: shear stiffness of springs; EJ and EA: bending and normal stiffness of the support; X and Y are the global Cartesian coordinates.

The active pressures

The HRM approach can be generalized for both shallow and deep tunnels. In the case of deep tunnels, when the overburden thickness is twice larger than the span/width (B) of the

tunnel, the active vertical load σ_v can be estimated using Terzaghi's formula [17]. An effective overburden thickness h_0 is determined by means of the following formula (see Figure 2):

$$h_0 = \frac{B_1\left(1-\left(c/B_1\gamma\right)\right)}{K_0\tan\phi}\left(1-e^{-K_0\tan\phi\left(H/B_1\right)}\right)+\frac{P_0}{\gamma}\left(e^{-K_0\tan\phi\left(H/B_1\right)}\right) \quad (1)$$

$$B_1 = B + H_t cot\left(\frac{(\pi/4)+(\varphi/2)}{2}\right) \quad (2)$$

$$\sigma_v = \gamma h_0 \quad (3)$$

where c, ϕ and γ are the cohesion, internal friction angle and unit weight of the ground, respectively; K_0 is the lateral earth pressure coefficient and H is the overburden to the tunnel crown, B and H_t are, respectively, the width and height of the tunnel; P_0 is the overload on the ground surface; γ is the unit weight of ground (MN/m³).
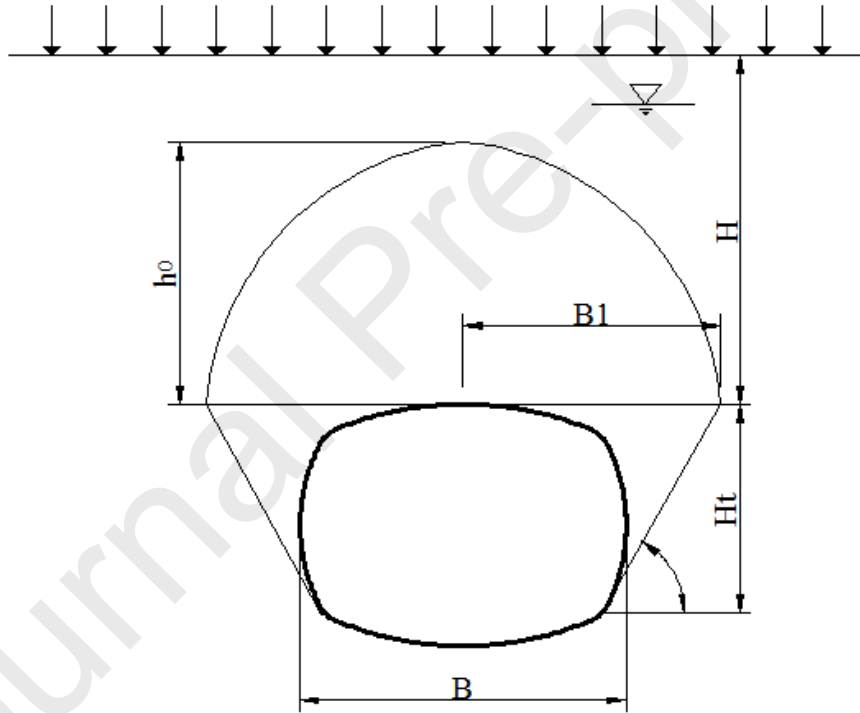

Figure 2. The overburden thickness h_0 determined by the Terzaghi's formula.

In the case of shallow tunnels, when the overburden depth is twice less than the tunnel diameter, the active vertical load σ_v can be estimated considering the change in depth over the tunnel height.

$$\sigma_{v(i)} = \gamma z_i \quad (4)$$

where z_i is the depth from the ground surface to the ground pressure level calculation (node i of the tunnel lining in HRM model) (m).

The horizontal pressure acting on the tunnel lining σ_h is determined on the basis of vertical loads:

$$\sigma_{h(i)} = K_0 \sigma_{v(i)} \tag{4}$$

where K_0 is the lateral earth pressure coefficient.

The ground-support interaction

The ground interacts with the tunnel support via normal and tangential springs connected to the nodes of the lining structure (see Figure 3) which are represented by k_n and k_s, respectively. The values of normal springs (k_n) and tangential springs (k_s) could be estimated based on the normal ground stiffness (η_n) and the tangential ground stiffness (η_s).
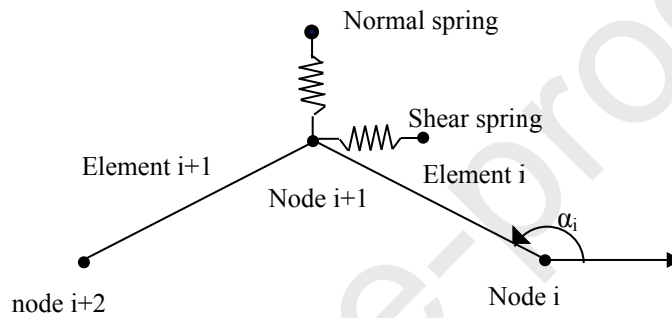

Figure 3. Details of the ground-support interaction through the Winkler springs connected to the support nodes

In the case of the squared tunnel and sub-rectangular tunnel in which radii of lining parts along the tunnel boundary are varied, the initial stiffness of the ground η_0 (when the tunnel displacement δ is close to 0) will change depending on the radius of parts of tunnel boundary:

$$\eta_{n,0(j)} = 2\frac{1}{1+v}\frac{E}{R_i} \tag{5}$$

where v and E are Poisson's ratio and Young's modulus, respectively, of the ground; R_i = radius of part i ($i=1$, 2 and 3 which corresponds to the crown, shoulder and side wall of the tunnel boundary).

3. Validation of HRM for the case of sub-rectangular tunnel

The undrained behavior of a sub-rectangular tunnel in clay is investigated in this study. The segment design of this tunnel was based on the silty clay soil stratum of Shanghai. As shown in Figure 4, the cross-section of the special-shaped shield tunnel is composed of eight arcs: top and bottom arcs, left and right arcs and four angle arcs. The ring is divided into six blocks: one seal roof block (F), two adjacent blocks ((L1 and L2) and three standard blocks (B1, B2, and B3). The segmental ring was cast by steel fiber reinforced concrete. Each ring has an inner

dimension of 10.2m×7.7m with a thickness of 0.5m and a width of 1.2m. The segments are fabricated by the staggered joint assembling method to enhance the longitudinal rigidity. The six segmental blocks are hinged circumferentially using six bolts, while the neighboring rings are connected by 26 bolts in the longitudinal direction.
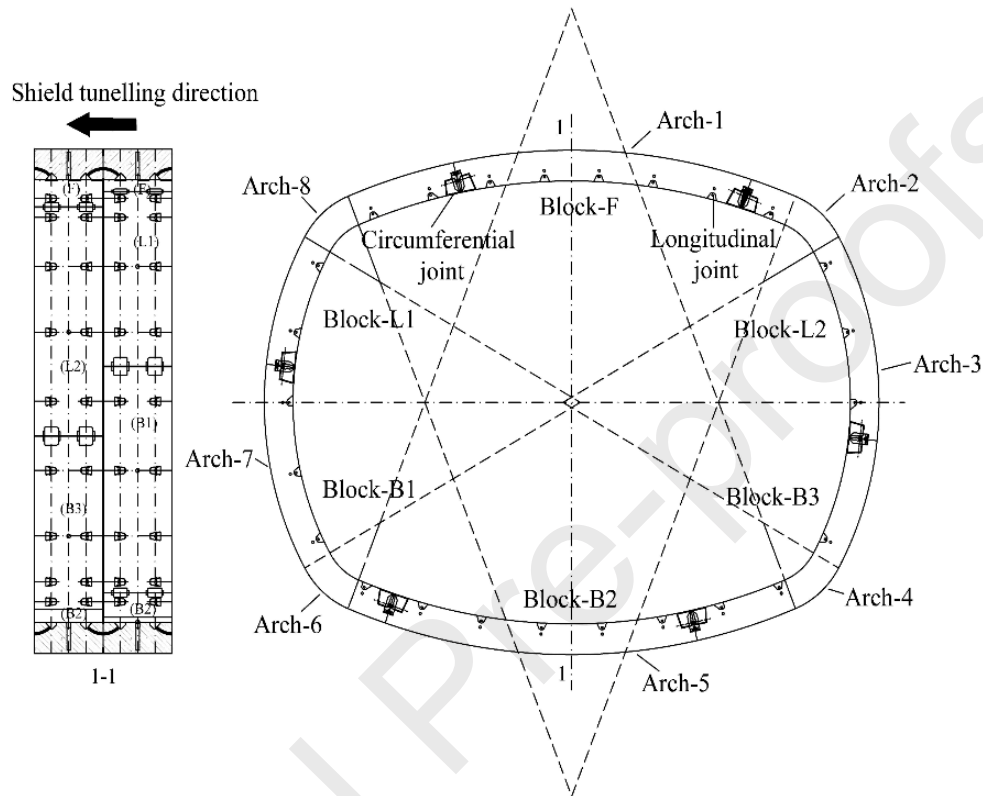

Figure 4. Segment layout of shield tunnel lining with a special-shaped cross-section

Parameters of one express tunnel in Shanghai, China are used as a reference case in this study. The dimensions of the sub-rectangular tunnel setup are 9.7m in width and 7.2m in height (Figure 5). The tunnel is located at a depth of 10m below the ground surface and is excavated in a silty clay soil which geotechnical parameters as mentioned in Table 1. A surcharge load of 20 kN/m^2 is assumed to be uniformly applied on the ground surface representing the surface loads. The tunnel is supported by a concrete lining whose thickness is equal to 0.5m. Parameters of the tunnel lining are summarized in Table 1. For the sake of simplicity, a continuous lining was adopted in this study without considering the effect of joints.

For a validation purpose of the HRM model, two cases of soil are assumed: (1) Case 1 in which the soil cohesion is constant, and (2) Case 2 where the soil cohesion is assumed to vary linearly with depth (Figure 5).

Table 1. Input parameters for the reference case

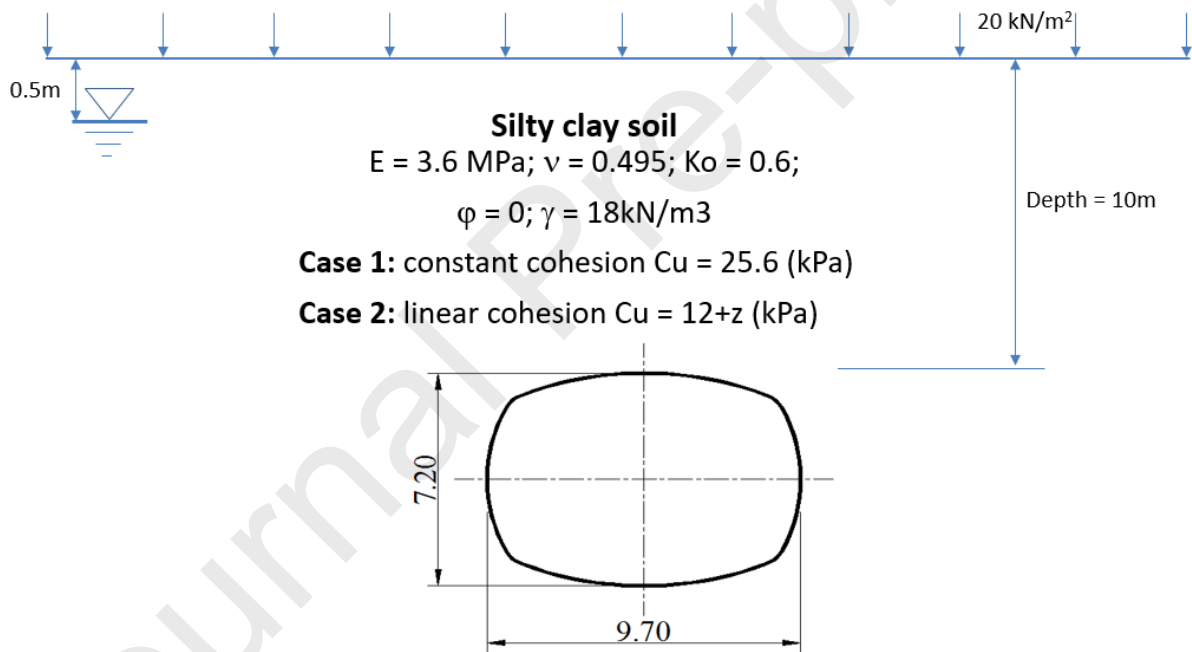| Parameter	Symbol	Value	Unit
Properties of silty clay soil			
Unit weight	γ	18	kN/m^3
Young's modulus	E	3.6	MPa
Poisson's ratio	ν	0.495	-
Internal friction angle	ϕ	0	degree
Cohesion	Cu	25.6	kPa
Lateral earth pressure coefficient	K_0	0.6	-
Overburden	H	10	m
Properties of tunnel lining			
Young's modulus	E_l	35,000	MPa
Poisson's ratio	ν_l	0.15	-
Lining thickness	t_l	0.5	m

Figure 5. Layout of the studied express tunnel

3.1. Numerical analysis of sub-rectangular tunnel using Plaxis^{2D} model

The performance of the HRM method for sub-rectangular tunnel design is estimated in this section on the basis of a comparison with the finite element method Plaxis^{2D}. The parameters shown in Table 1 and Figure 5 were adopted for this evaluation. A plane strain model was created with the Plaxis^{2D} [2]. The behavior of the tunnel structure is assumed to be linear elastic and the ground one is governed by a linear elasto-plastic Mohr-Coulomb constitutive model [17,22], which is degraded into a Tresca model for the case of a zero friction angle. Considering

this simple soil constitutive model does not permit to follow the real soil behavior, the main idea of this research is in fact to evaluate the ability of the HRM method compared to a 2D numerical model for the preliminary design of tunnel linings.

The soil medium is discretized into 15-noded elements. The tunnel lining is modelled by using plate elements with an interface between the plate and the soil. In order to model the soil-structure interaction, an interface was added between the plate and the soil. This interface is used to simulate the thin shearing zone at the contact between the plate and the surrounding soil. The material properties of the interface are taken equal as the surrounding soil ones [2].

The numerical model (Figure 6) is 100 m wide in the x-direction, 55 m high in the y-direction and consists of approximately 7,400 zones and 59,000 nodes. The bottom of the model was fixed in the vertical direction and the vertical sides were fixed in the horizontal one. The gravity effect was considered in this study.

For the simulation process, the following phases have been adopted:

Phase 0 - Set up the model: setting up the model and assigning boundary conditions and the initial stress state;

Phase 1 - Excavation phase: The excavated ground inside the tunnel boundary is deactivated. It should be mentioned that the soil relaxation after the excavation and before the lining installation was not considered. All the external loads caused by the ground were applied to the lining in order to consider the worst case of the lining stress.

Phase 2 - Installation of the tunnel support: the tunnel lining is activated on the tunnel boundary.
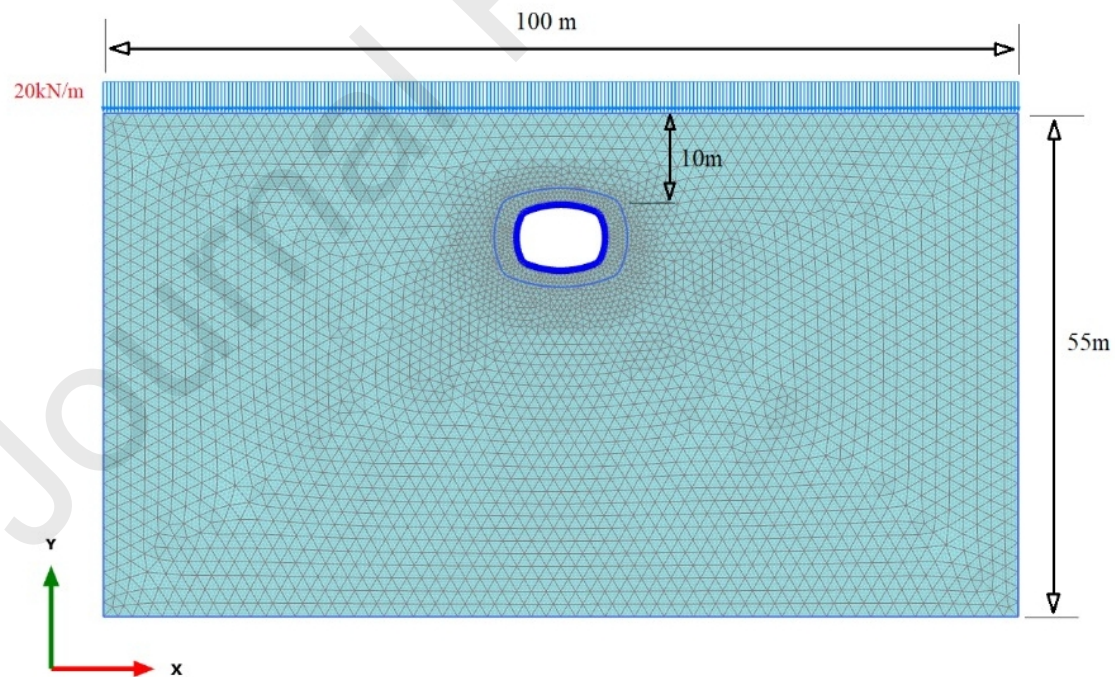
Figure 6. Finite element geometry and mesh

### 3.2. Comparison between HRM and Plaxis^{2D} results

Two soil cases are considered: a) the soil stratum is homogeneous and has a constant cohesion; b) the cohesion varies linearly with the burial depth. The internal forces induced in

the tunnel lining obtained by using the HRM model and a finite element model (Plaxis), for the two soil cases, are respectively compared in Figure 7 and Figure 8. In order to highlight the tunnel shape effect and for the comparison purpose, the internal forces induced in the circular tunnel having the same cross-section area are also presented. The results show that the HRM model gives results in terms of bending moments and normal forces obtained in the case of sub-rectangular shaped tunnels which reasonably agree well both in distribution and magnitude with those of Plaxis^{2D} model for both cases of soil mediums.

As for case 1 (constant cohesion of soil), Figure 7 and Table 2 indicate small differences for the maximum and minimum bending moments obtained by the HRM model and the finite element model (Plaxis). These differences are respectively equal to 8.21% and 3.39%. The HRM model gives the maximum and minimum normal forces which are 8.84% and 9.54%, respectively, smaller than those of the Plaxis^{2D} model. The difference between results of the HRM model and Plaxis^{2D} model in terms of internal forces can be explained by the soil/structure interaction simulation (soil and tunnel lining). Indeed, while an explicit simulation of the soil medium is used in Plaxis^{2D} which allows a realistic interaction between soil and tunnel lining could be considered, normal and tangential springs with stiffnesses are used in the HRM model to represent the soil medium. The same tunnel lining behavior can be seen for case 2 where the soil cohesion varies linearly with depth (Figure 8 and Table 2). However, the effect of varying the cohesion on the lining behavior is insignificant in the considered cases. On the basis of the above analysis, it is reasonable to conclude that the HRM model can effectively be used to evaluate the structural forces induced in the sub-rectangular tunnel lining.

It should be mentioned that the bending moment distribution pattern induced in the sub-rectangular tunnel is slightly different from the one observed in the experimental tests conducted by Nakamura et al. [11], Xian et al. [18]. They showed that the largest negative bending moment occurs nearly at the four corners. The difference between the Plaxis model and HRM model performed in this study and the experimental data can be attributed to the presence of joints in the linings which are not considered in the proposed numerical models. The distribution of bending moments at the joints level is modified as there are two joints located closely to the two waists in Figure 4.

Figures 7 and 8 indicate also a strong influence of the tunnel shape on the tunnel lining behavior in terms of bending moment and normal forces. As predicted, circular tunnel gives bending moments (M) and normal forces (N) which are smaller than those observed in the case of sub-rectangular tunnels. The difference in the radius or flatness of the parts along the tunnel boundary cause a modification of the transferring mechanisms for the axial forces inside the tunnel lining and a change in the reaction forces from the soil surrounding the tunnel acting on the lining. In addition, the difference in the width/span of the tunnel between the tunnel cases can also leads to a change in terms of external loads applied to the lining. As a consequence, structural forces induced in the tunnel lining are greatly affected by the tunnel shape.
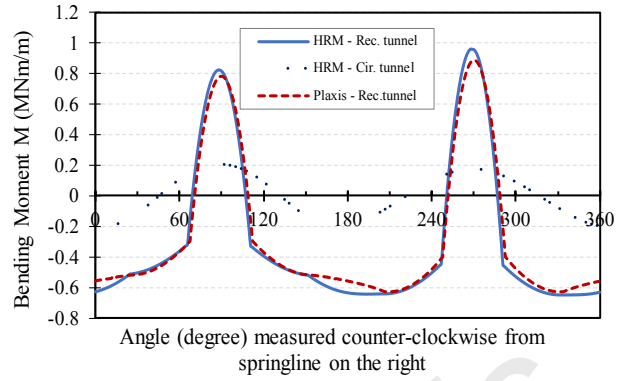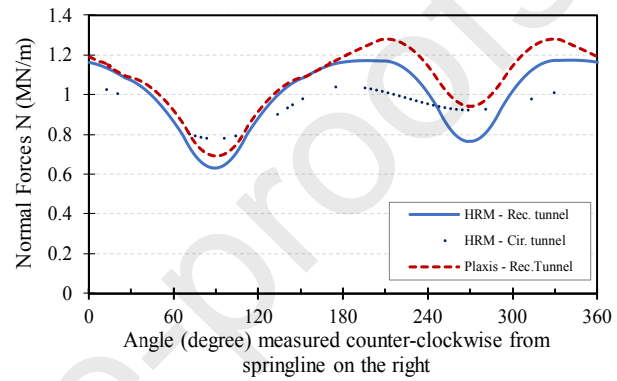
a) Bending moment M
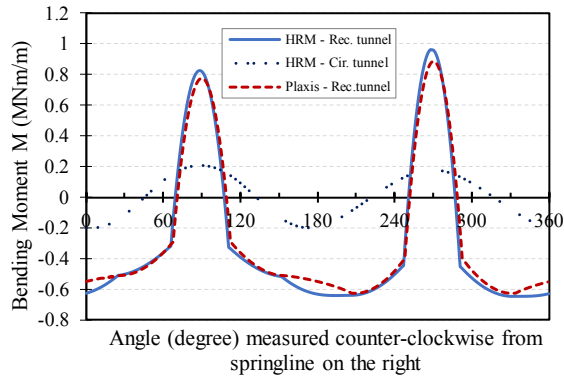
a) Bending moment M
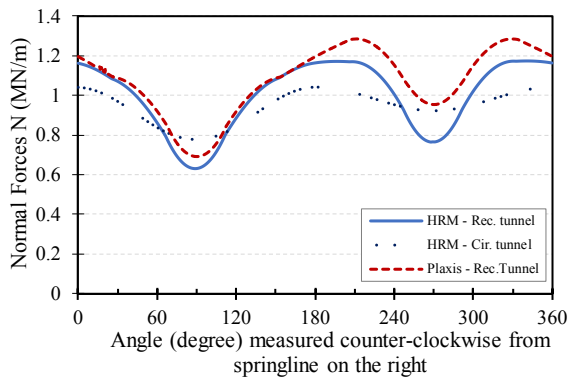
b) Normal Forces N

b) Normal Forces N

Figure 7. Internal forces induced in the tunnel lining (case 1)

Figure 8. Internal forces induced in tunnel lining in the case of soil's cohesion varied in depth (case 2)

Table 2. Internal forces induced in the tunnel lining

Case	Values	M (MN.m/m)			N (MN/m)		
		HRM model	Plaxis[2D] model	Difference (%)	HRM model	Plaxis[2D] model	Difference (%)
Case 1	Maximum	0.962	0.883	8.21	1.176	1.28	-8.84
	Minimum	-0.649	-0.627	3.39	0.629	0.689	-9.54
Case 2	Maximum	0.964	0.888	7.88	1.176	1.28	-8.84
	Minimum	-0.650	-0.628	3.38	0.631	0.692	-9.67

4. Parametric study

The aim of this section is to investigate the tunnel shape influence on the lining behavior in terms of structural forces and radial lining deformation induced by the tunnel excavation. The radii of parts along the tunnel boundary (R1, R3, and R2) respectively correspond to the radius of the top and bottom parts, side walls and shoulder of tunnels (Figure 9) are modified from case to case. It should be noted that the tunnel boundary is symmetrical over both the

vertical and horizontal tunnel axes. In total 8 tunnel shape cases are considered. Studied cases are divided into two groups: (1) squared tunnel in which the width and height of the tunnel are the same, (2) sub-rectangular tunnel where the width of the tunnel is larger than the height. The excavation area of all tunnel cases is the same and equal to the reference case one (59.8 square meters). The case of a circular tunnel with the same excavation area is considered for the comparison purpose. The adopted radii of the parts along the tunnel boundary for each tunnel shape case are presented in Table 3. Only the HRM model was used in this section. Due to the low difference between case 1 and case 2 reported before, the soil parameters of Case 1 (constant soil cohesion) were used for the following study (Figure 5).

A parametric study to investigate the influence of the lateral earth pressure coefficient (K_0) and of the Young's modulus (E) of soil is proposed. The K_0 values are assumed to vary in a range between 0.4 and 1.0 (while the soil deformation modulus is kept as 3.6 MPa). The Young's modulus of soil is assumed to be in the range between 1 and 20 MPa (while keeping $K_0 = 0.6$).

Table 3. Geometrical parameters of tunnel shape cases

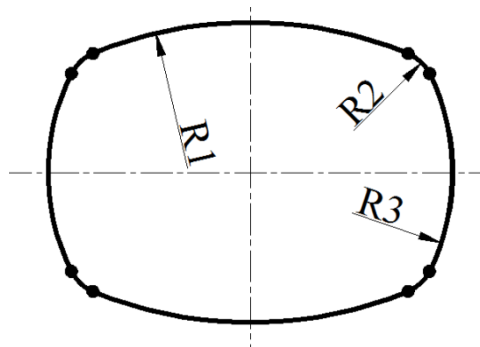| Case	Tunnel width (B) (m)	Tunnel height (H_t) (m)	B/H_t ratio	R1 (m)	R2 (m)	R3 (m)	Area (m^2)	Type of tunnel shape
S0 (reference case)	8.72	8.72	1.000	4.36			59.786	Circular
S1	8.6	8.55	1.006	5.47	3.67	5.47	59.759	
S2	8.45	8.37	1.010	6.56	1.23	6.56	59.795	Squared
S3	8.20	8.20	1.000	9.88	0.85	9.88	59.812	
SR1	8.76	8.15	1.075	8.36	1.02	4.99	59.788	
SR2	9.13	7.89	1.157	7.09	1.23	4.81	59.757	Sub-
SR3	9.39	7.53	1.247	8.50	0.96	5.07	59.778	rectangular
SR4	9.70	7.20	1.347	9.95	1.00	5.35	59.786	

Figure 9. Definition of the radius in squared and sub-rectangular tunnels

S0

8.15

8.76

SR1

8.55

8.60

S1

7.89

9.13

SR2

8.37

8.45

S2

7.53

9.39

SR3

8.20

8.20

S3

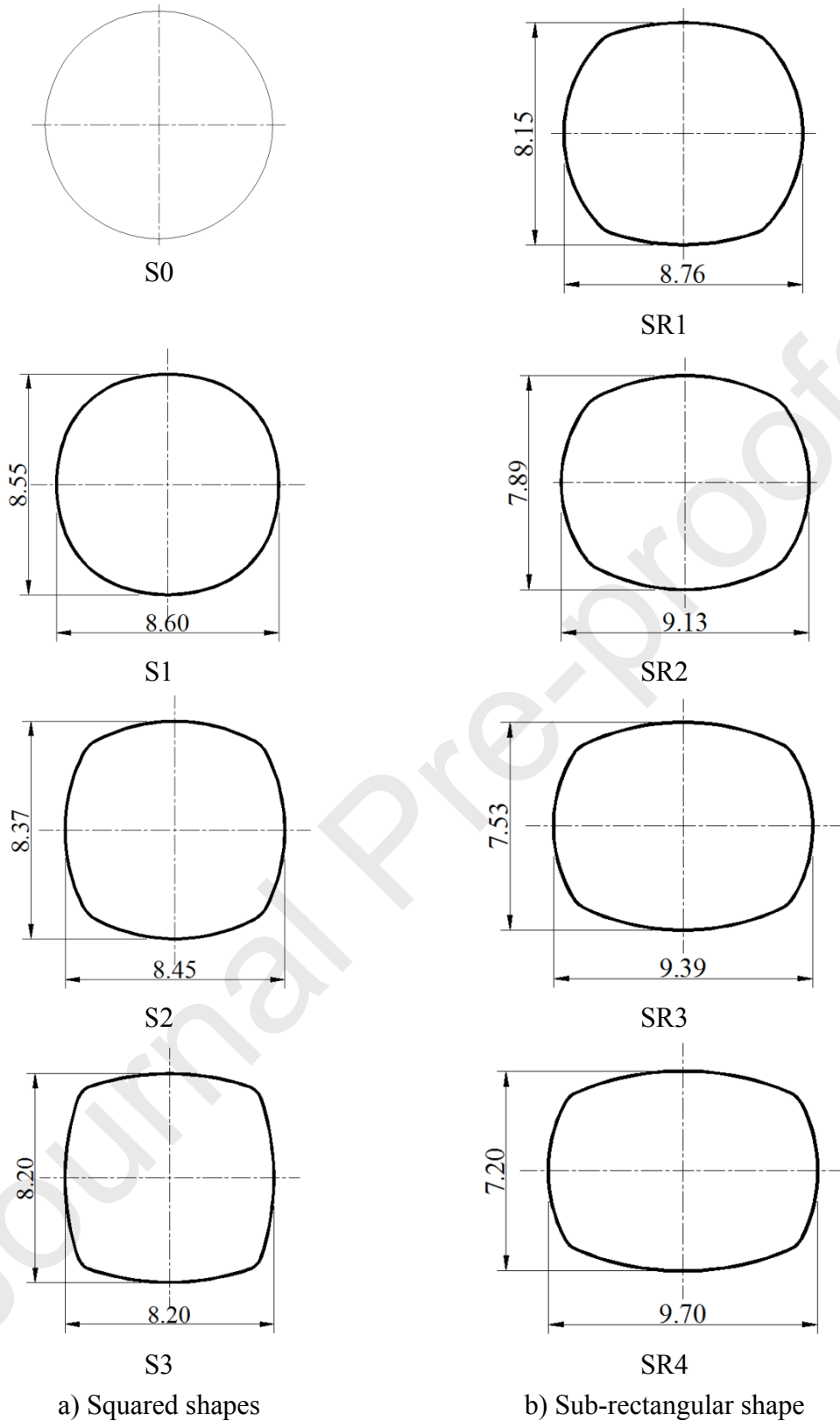7.20

9.70

SR4

a) Squared shapes

b) Sub-rectangular shape

Figure 10. Shapes of tunnel cases (unit: m)

## 4.1. Influence of the tunnel shape on the tunnel lining behavior

Results of structural forces and normal displacements induced in the tunnel lining are presented in Figure 10, Figure 11 and Table 4. For the sake of simplicity, the results are separately introduced for squared tunnels and sub-rectangular tunnels. As predicted, structural forces induced in a circular tunnel are smaller if compared to other cases of tunnel shapes, i.e. squared tunnels and sub-rectangular tunnel (Table 4).
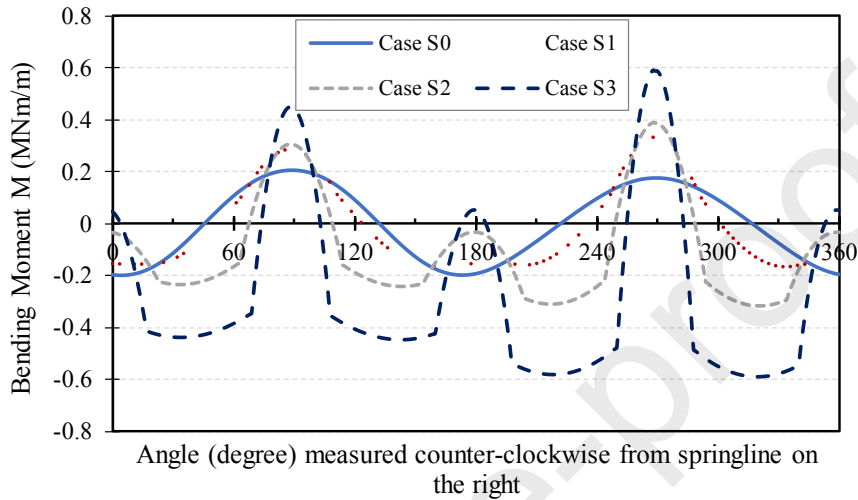
a) Bending moment M
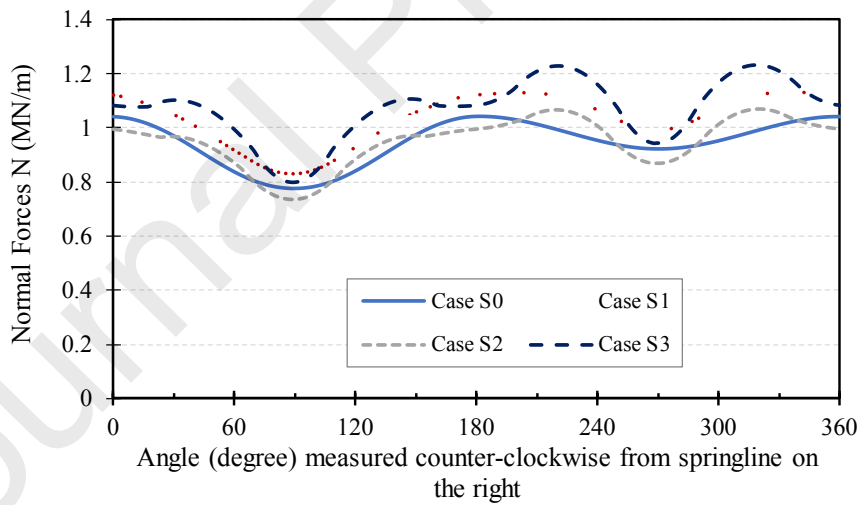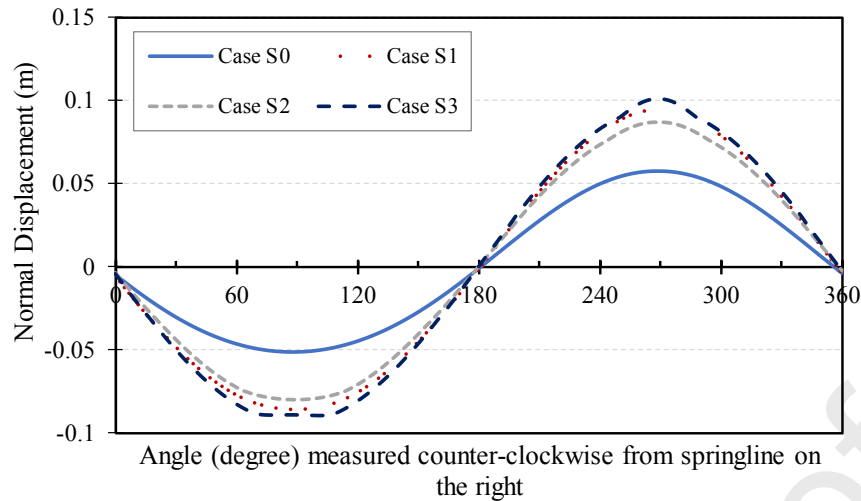
b) Normal Forces N

c) Normal Displacement

Figure 11. Internal forces and normal displacement induced in the squared tunnel linings

As for squared tunnels, when the radius of the top and bottom parts and the side walls of the tunnel increases, which means a decrease of the shoulder parts radius, the bending moment, normal forces and normal displacements in the tunnel lining generally increase. In other words, an increase in the smallest radius of the tunnel lining parts, i.e. the R2 radius, will be followed by a decrease of the structural forces and normal displacement of the lining. This observation is in good agreement with the fact that when the tunnel lining sections are flatter, i.e. varying from case S1 to S3, the maximum induced bending moments are higher in the middle of the section as seen at the crown and bottom of the tunnel lining (Figure 11a). It should be mentioned that the higher bending moments are also observed at the shoulders of the tunnel lining where the tunnel boundary radius is smaller compared to other parts. The smaller the radius of the shoulder parts, i.e. varying from case S1 to S3, the higher the minimum bending moment. It is interesting to note that the absolute value of the negative bending moment induced at the spring line of the squared tunnel is smaller than the circular case one. Unlike for bending moments, the changes of normal forces caused by the change of shape of squared tunnels are mainly located at the tunnel shoulders where the radius R2 is smaller than the R1 and R3 radii. An increase in the normal forces at these positions is observed as seen in Figure 11b.

The effect of sub-rectangular tunnel shapes on the tunnel lining behavior is shown in Figure 12. Higher radii of the top and bottom (R1), and side walls (R2); which also mean lower shoulder radius (R3), will cause an increase of the bending moments along with all the tunnel boundary. It means that the behavior of the sub-rectangular tunnel lining in terms of bending moments is different from the behavior of squared tunnels mentioned above. Indeed, Figure 12a and Table 4 show an increase of the negative absolute bending moments value at the side walls of sub-rectangular tunnels.

Nevertheless, while an increase of normal forces at the side walls can be seen in Figure 12b, a decrease of the normal forces is observed at the top and bottom of the tunnel lining. This decrease of normal forces at the top and bottom of the tunnel when these parts of the sub-rectangular tunnel are flatter could be explained by the transmission of forces decrease from the side walls and shoulder parts due to the lower arching effect in the lining.

Table 4. Results of the structural forces and normal displacements induced in the tunnel lining

| N^0	Case	M_{max} (MNm/m)	Diff. (%)	M_{min} (MNm/m)	Diff. (%)	N_{max} (MN/m)	Diff. (%)	N_{min} (MN/m)	Diff. (%)	δ_{max} (m)	Diff. (%)	δ_{min} (m)	Diff. (%)
1	S0 Ref. case	0.21		-0.20		1.04		0.78		0.06		-0.05	
2	S1	0.33	59.5	-0.17	-15.9	1.13	9.0	0.83	6.9	0.09	63.5	-0.09	66.8
3	S2	0.39	87.6	-0.31	58.7	1.07	2.8	0.74	-4.9	0.09	50.2	-0.08	55.4
4	S3	0.59	183.7	-0.59	196.4	1.23	18.3	0.80	2.9	0.10	74.9	-0.09	74.1
5	SR1	0.57	176.0	-0.26	29.4	1.11	6.9	0.74	-4.0	0.09	60.8	-0.08	54.6
6	SR2	0.69	230.2	-0.44	121.6	1.17	12.6	0.73	-5.7	0.09	61.2	-0.07	41.1
7	SR3	0.86	315.3	-0.56	182.8	1.20	15.7	0.70	-10.3	0.09	62.8	-0.07	37.0
8	SR4	0.96	362.7	-0.65	226.9	1.18	13.0	0.63	-18.8	0.10	66.9	-0.07	39.1

(Note: Diff. means difference)
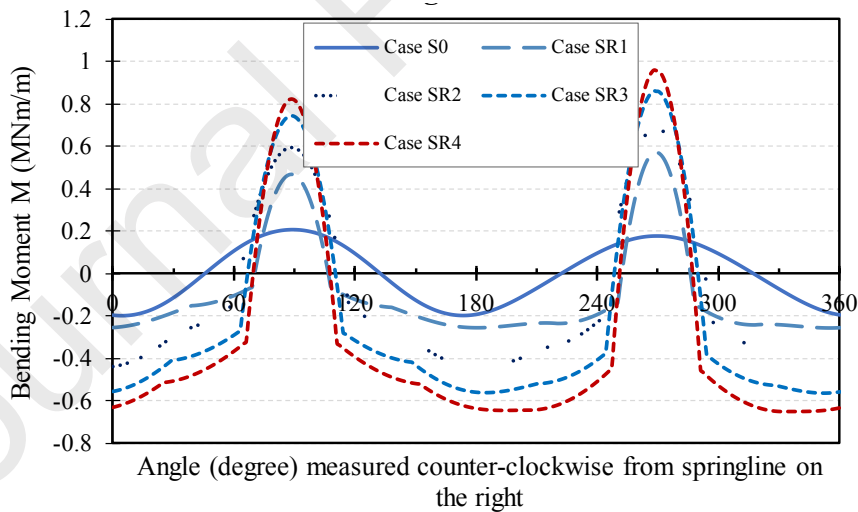
a) Bending moment M
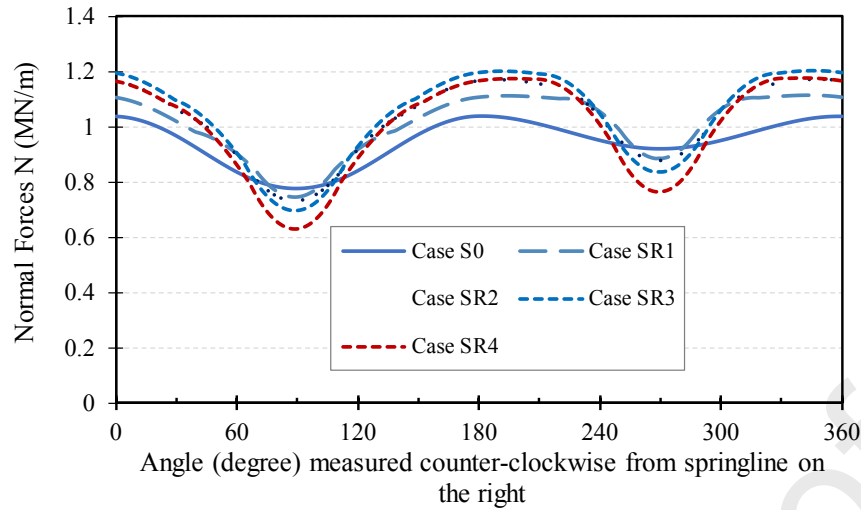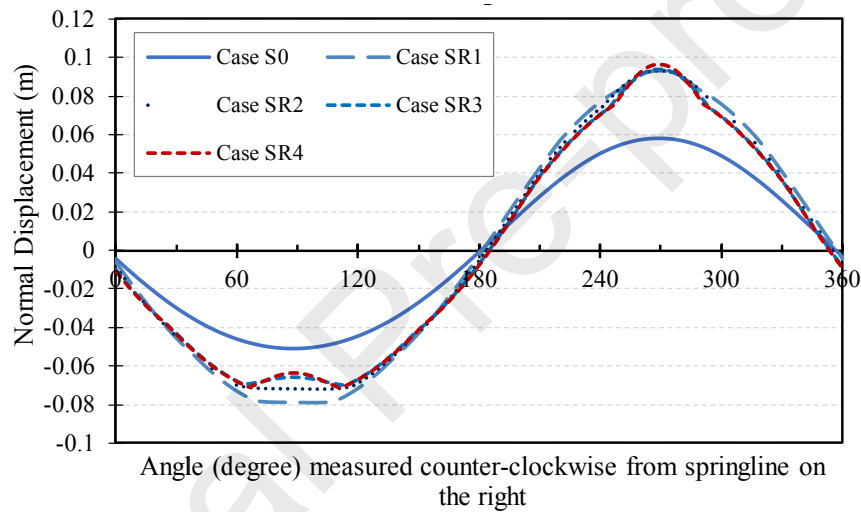
b) Normal Forces

c) Normal Displacement

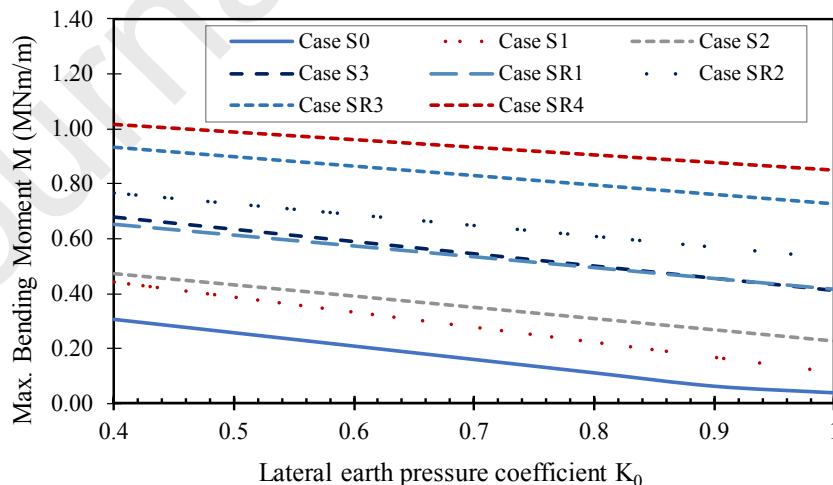Figure 2. Internal forces and normal displacements induced in the sub-rectangular tunnel linings

On the basis of the above analysis, it is reasonable to conclude that, for the case of K_0 value of 0.6 considered in this section, squared tunnels are more stable than sub-rectangular tunnels in terms of structural forces induced in the lining. It is in good agreement with the technical recommendation that the longer axis of the tunnel cross section should be placed in the direction of the primary loadings. In the case of the sub-rectangular tunnels considered in this study, the longer axis of the tunnel cross section is perpendicular to the vertical loadings which are the primary ones. Consequently, sub-rectangular shapes will lose stability more easily than the squared ones. The most suitable squared tunnel shape is Case S1. It is also interesting to note that when using sub-rectangular tunnels, the smaller the difference between the height and width of the tunnel is and the smaller the structural forces induced in the tunnel lining are.

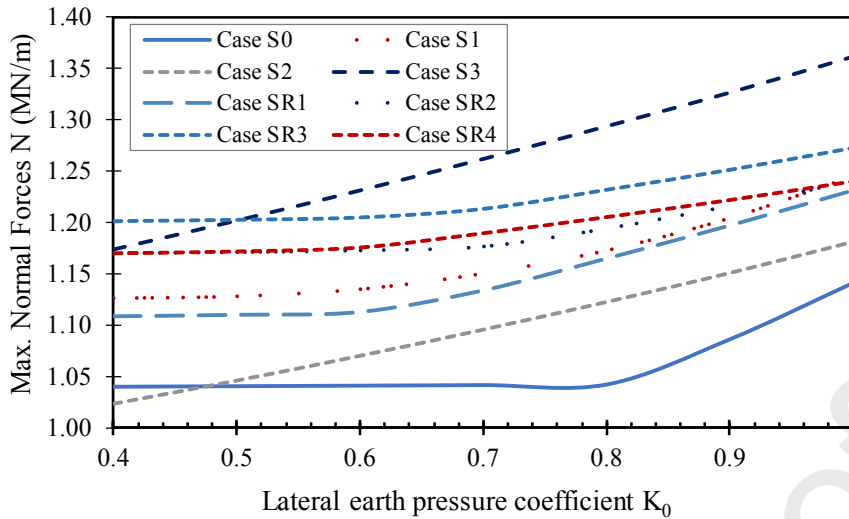## 4.2. Effect of the lateral earth pressure coefficient K_0

An extensive parametric analysis is developed to investigate the effect of the lateral earth pressure coefficient K_0 on the tunnel lining behavior in terms of bending moment (M), normal forces (N) and normal lining displacements values (δ_n). The K_0 value is assumed to be in the range between 0.4 and 1.0 which covers most of the range of the lateral earth pressure coefficient in reality. The other parameters of Case 1 (constant soil's cohesion) are adopted in this section.

The results from these parametric analyses permitted to draw Figure 13, Figure 14 and Figure 15. The following conclusions can be drawn:
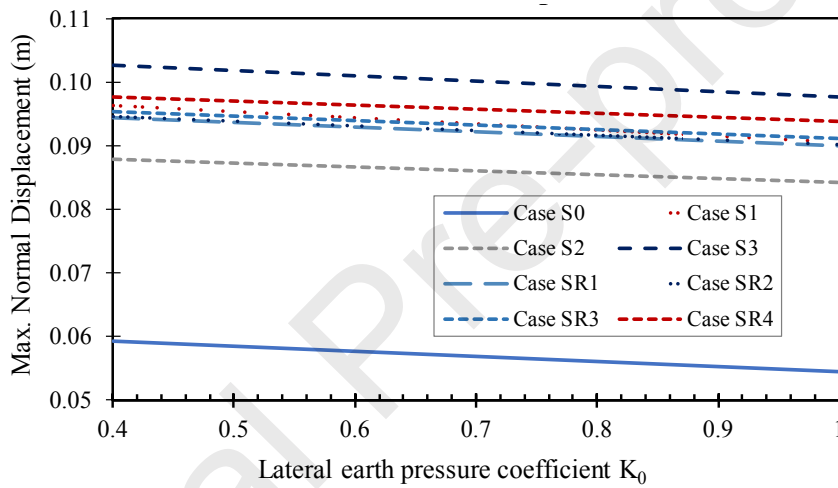
• The higher the lateral earth pressure coefficient, the lower the maximum bending moment and normal displacement but the greater the maximum normal forces (see Figure 13Figure). This is observed for both squared and sub-rectangular tunnels. In other words, both squared tunnels and sub-rectangular tunnels will be more stable when being placed in soils of high K_0 values. In addition, the maximum bending moment is generally linearly dependent on the lateral earth pressure coefficient K_0 (Figure 13a);

• The dependence of the maximum normal forces in the squared tunnel lining is not like the sub-rectangular ones. While the maximum normal forces are linearly dependent of the lateral earth pressure coefficient K_0, the maximum normal forces induced in sub-rectangular tunnels are nearly constant when the K_0 value is smaller than 0.6 (Figure 13b);

• As predicted, when keeping the K_0 value constant, a tunnel width increase will cause greater maximum bending moments. A linear dependency of the maximum bending moment on the crown part radius of squared tunnels or tunnel width in sub-rectangular tunnels is respectively observed in Figure 14 and Figure 15.

(a) Maximum Bending moment M_{max}

b) Maximum Normal Forces N_{max}

c) Maximum Normal Displacement

Figure 3. Effect of the lateral earth pressure coefficient (K_0) on the internal forces and normal displacements induced in the tunnel lining
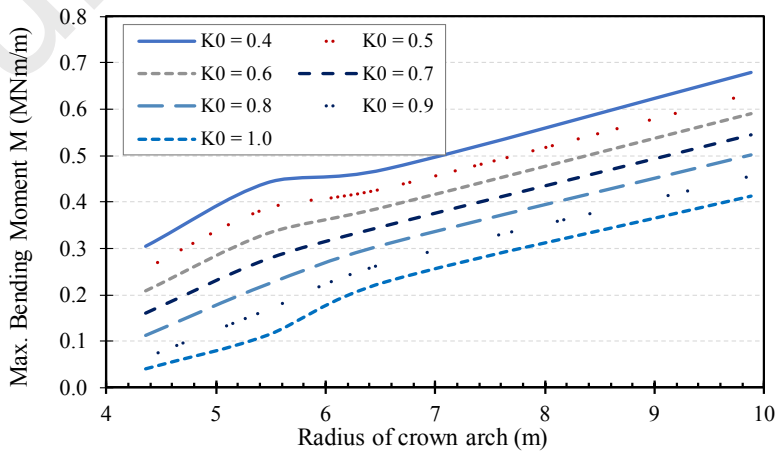

Figure 14. Effect of the crown arch radius on the Maximum Bending moments induced in squared tunnel lining considering the K_0 value variation
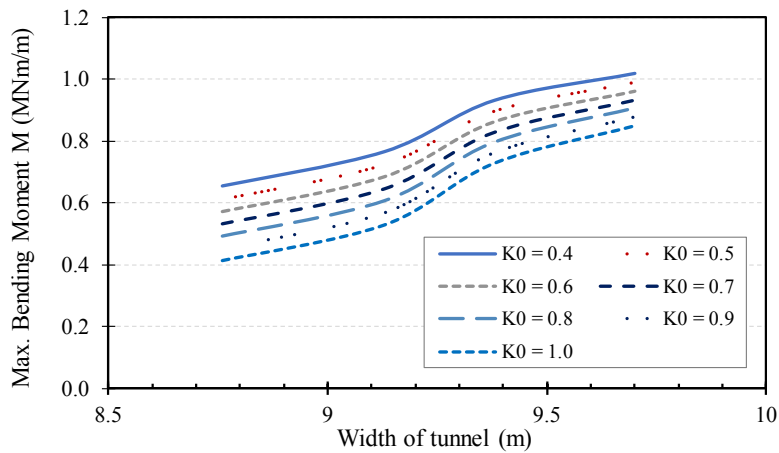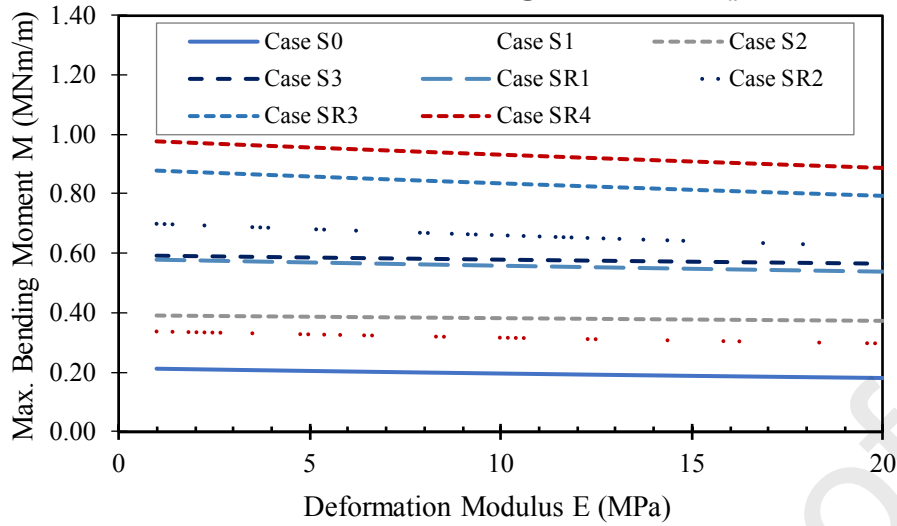
Figure 15. Effect of the tunnel span on the Maximum Bending moment induced in sub-rectangular tunnel lining considering the K_0 value variation

4.3. Effect of Young's modulus (E)

Young's modulus values for the soil are assumed to be in the range from 1 to 20 MPa while keeping K_0 equal to 0.6. The other parameters for the soil are the ones of Case 1 (constant soil's cohesion). The numerical results obtained using the HRM model are presented in Figure 16, Figure 17 and Figure 18. Based on these figures, it can be said that:

- With small E values considered, insignificant effects on the bending moments and normal forces in the tunnel lining can be observed in Figure 16a and b;

- Unlike for the bending moments and normal forces, induced normal displacements are strongly dependent on the E values (Figure 16c). Indeed, for low range values of E (E ≤ 4 MPa), the increase of the E value is followed by the decrease of normal displacements. However, for larger values of modulus E, no dependency of the normal displacements on Young's modulus can be observed;

- When keeping the E value constant, an increase of the crown part radius of squared tunnels or of the tunnel width of sub-rectangular tunnels causes a greater maximum bending moment (Figure 17 and Figure 18, respectively).

(a) Maximum Bending moment M_{max}
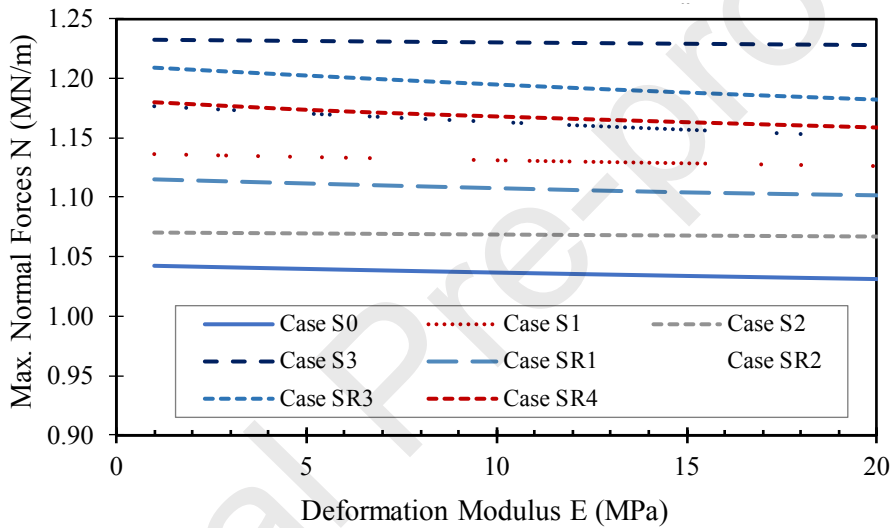
b) Maximum Normal Forces N_{max}
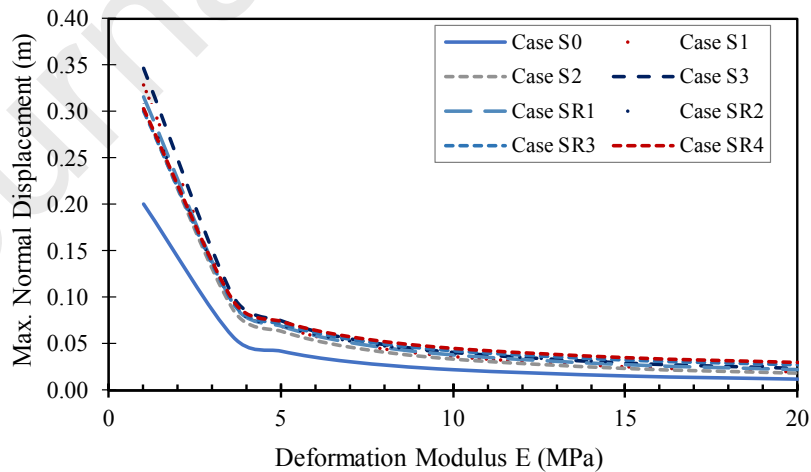
c) Maximum Normal Displacement

Figure 16. Effect of the E value on the internal forces and normal displacements induced in squared and sub-rectangular tunnel lining
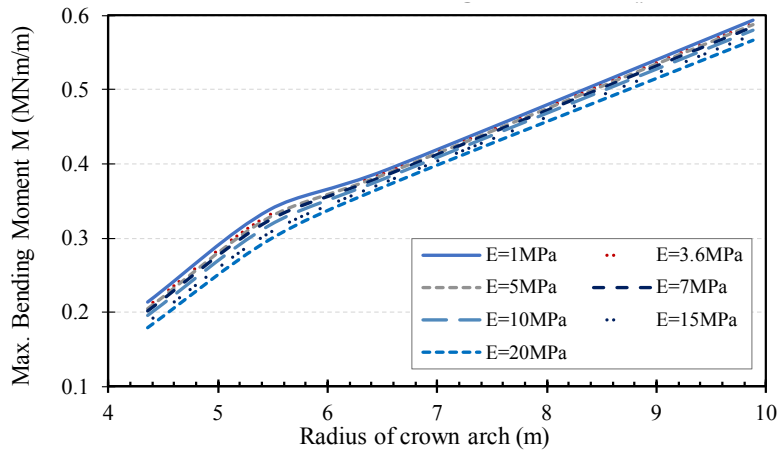
Figure 17. Effect of the crown radius arch on the Maximum Bending moment induced in squared tunnel lining considering the change of E values
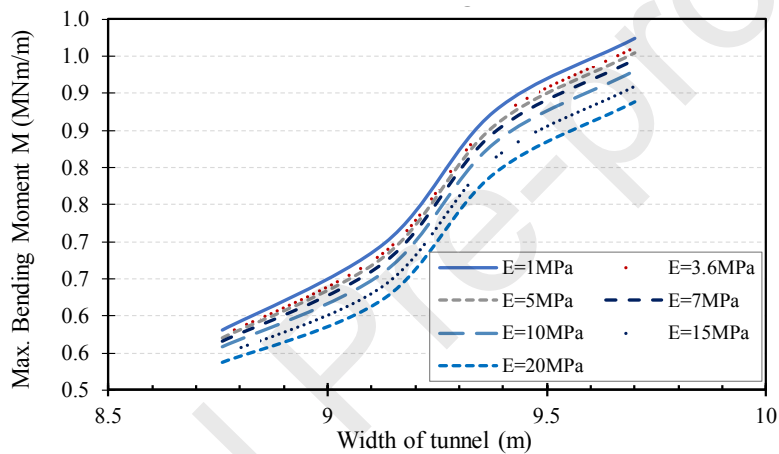

Figure 18. Effect of tunnel span on the Maximum Bending moment induced in sub-rectangular tunnel linings considering the change of E values

5. Conclusions

The HRM model is particularly effective to estimate the tunnel lining behavior in terms of structural forces and deformations. An improvement of the HRM numerical model was made to apply to squared and sub-rectangular tunnels. A comparison with numerical results applied to the case of an express tunnel allowed the developed HRM model to be validated for complex tunnel shapes.

An extensive parametric analysis was performed to highlight the effect of the tunnel shape on the lining behavior. On the basis of the parametric study using the HRM model, it is reasonable to conclude that, for the case of a K_0 value of 0.6 considered in this study, squared tunnels are more stable than sub-rectangular ones in terms of structural forces induced in the lining. The most suitable shape for squared tunnels is observed in Case S1 (Figure 10 and Table 3). When using sub-rectangular tunnel, the smaller the difference between the height and width of the tunnel is, the smaller the structural forces induced in the tunnel lining are.

A significant dependency of the structural forces and lining deformations on the K_0 value is presented. Accordingly, both squared and sub-rectangular tunnels are more stable when located in soils with high K_0 values. However, while the maximum normal forces are linearly dependent on the lateral earth pressure coefficient K_0, the maximum normal forces induced in sub-rectangular tunnels are nearly constant when the K_0 value is smaller than 0.6.

A numerical investigation using the HRM model also indicated that in case of small Young's soil modulus, an insignificant effect of the E value on the bending moments and normal forces in the tunnel lining is predicted.

In conclusion, this study shows a great effect of the tunnel shape on the tunnel lining behavior. To enhance the stability of the tunnel lining (lower structural forces), the longer axis of the tunnel cross section should be placed in the direction of the primary external loadings. In addition, it is suggested to avoid using higher radius or flatness of the parts along the tunnel boundary which will cause a decrease of the transferring mechanism from point to point of the axial forces inside the tunnel lining and a change in the reaction forces from the soil surrounding the tunnel acting on the lining.

References

[1] Blom CBM. Design philosophy of concrete linings for tunnels in soft soils. Ph.D. Thesis, Delft University of Technology 2002.

[2] Brinkgreve RBJ. Plaxis: finite element code for soil and rock analyses. Balkema, 2002.

[3] Do NA, Dias D, Oreste PP. The behaviour of the segmental tunnel support studied by the hyperstatic reaction method. European Journal of Environmental and Civil Engineering 2014a; 18(4): 489-510. doi: 10.1080/19 648189.2013.872583.

[4] Do NA, Dias D, Oreste PP & Djeran-Maigre I. A new numerical approach to the hyperstatic reaction method for segmental tunnel linings. International Journal for numerical and analytical methods in geomechanics 2014b; 38(15), 1617-1632.

[5] Huebner KH, Dewhirst DL, Smith DE & Byrom TG. The finite element method for engineers. John Wiley and Sons, inc., New York 2001.

[6] Kashima Y, Kondo N, Inoue M. Development and application of the DPLEX shield method: Results of experiments using shield and segment models and application of the method in tunnel construction. Tunnelling and Underground Space Technology 1996; 11(1):45-50.

[7] Konstantin PB, Mikhail OL. About rock pressure loads on tunnel linings constructed using trenchless method. Journal of Mining Institute2017; 228: 649-653.

[8] Liu X, Ye Y, Liu Z, Huang D. Mechanical behavior of Quasi-rectangular segmental tunnel linings: First results from full-scale ring tests. Tunn. Undergr. Space Technol. 2018a; 71, 440-454.

[9]   Liu X, Ye Y, Liu Z, Yun B, Yaohong Z. Mechanical behavior of quasi-rectangular segmental tunnel linings: Further insights from full-scale ring tests. Tunnelling and Underground Space Technology 2018b; 71, 440-453.

[10] Molins C, Arnau O. Experimental and analytical study of the structural response of segmental tunnel linings based on an in situ loading test: Part 1: Test configuration and execution. Tunnelling and Underground Space Technology 2011; 26(6): 764-777.

[11] Nakamura H, Kubota T, Furukawa M, et al. Unified construction of running track tunnel and crossover tunnel for subway by rectangular shape double track cross-section shield machine. Tunnelling and Underground Space Technology 2003; 18(2): 253-262.

[12] Oreste P. A numerical approach to the hyperstatic reaction method for the dimensioning of tunnel supports. Tunnelling Underground Space Technol. 2007; 22(2), 185-205.

[13] Oreste P, Spagnoli G and Ceravolo LA. A numerical model to assess the creep of shotcrete linings. Proceedings of the Institution of Civil Engineers - Geotechnical Engineering 2019; 172(4): 344-354.

[14] Oreste P, Spagnoli G and Luna Ramos CA. Evaluation of the safety factors of shotcrete linings during the creep stage. Proceedings of the Institution of Civil Engineers - Geotechnical Engineering 0 0:0, 1-9.

[15] Oreste P, Spagnoli G and Luna Ramos, CA. The Elastic Modulus Variation During the Shotcrete Curing Jointly Investigated by the Convergence-Confinement and the Hyperstatic Reaction Methods. Geotech Geol Eng 2019; 37, 1435-1452. doi:10.1007/s10706-018-0698-1.

[16] Oreste P, Spagnoli G, Luna Ramos, CA and Hedayat A. Assessment of the Safety Factor Evolution of the Shotcrete Lining for Different Curing Ages. Geotechnical and Geological Engineering 2019; doi: https://doi.org/10.1007/s10706-019-00990-2.

[17] Takano YH. Guidelines for the design of shield tunnel lining. Tunnelling and Underground Space Technology 2000; 15(3), 303-331

[18] Xin H, Yeting Z, Zixin Z, Yanfei Z, Shuaifeng W, Qianwei Z. Mechanical behaviour of segmental lining of a sub-rectangular shield tunnel under self-weight. Tunnelling and Underground Space Technology 2018; 74: 131–144.

[19] Zhang ZX, Zhu YT, Zhu YF, et al. Development and application of a 1:1 mechanical test system for special-shaped shield lining with a large cross-section. Chinese Journal of Rock Mechanics and Engineering 2017; 12(36): 2895-2905. (in Chinese)

[20] Zhu YT, Zhang ZX, Zhu YF, et al. Capturing the cracking characteristics of concrete lining during prototype tests of a special-shaped tunnel using 3D DIC photogrammetry. European Journal of Environmental & Civil Engineering 2017; 1-21.

[21] Zixin Z, Yeting Z, Xin H, et al. "Standing" full-scale loading tests on the mechanical behavior of a special-shape shield lining under shallowly-buried conditions. Tunnelling and Underground Space Technology 2019; 86(1): 34-50.

[22] Vinod M, Khabbaz H. Comparison of rectangular and circular bored twin tunnels in weak ground. Underground Space 2019; 4(4): 328-339.

Credit Author statement

Do Ngoc Anh: Investigation, Development of reliability algorithms, Calculations, Writing and Original draft preparation

Dias Daniel: Reviewing and Editing

Zixin Zhang: Conceptualization

Xin Huang: Methodology

Nguyen Tai Tien: Calculations

Pham Van Vi: Calculations

Ouahcène Nait-Rabah: Reviewing and Editing

Declaration of interests

☒ The authors declare that they have no known competing financial interests or personal relationships that could have appeared to influence the work reported in this paper.

☐The authors declare the following financial interests/personal relationships which may be considered as potential competing interests: